Current Optics and Photonics
Vol. 2, No. 4, August 2018, pp. 378-382

ISSN: 2508-7266(Print) / ISSN: 2508-7274(Online)
DOI: https://doi.org/10.3807/COPP.2018.2.4.378

Resonance Characteristics of THz Metamaterials Based on a Drude Metal with Finite Permittivity

Seung Won Jun and Yeong Hwan Ahn*

Department of Physics and Department of Energy Systems Research, Ajou University, Suwon 16499, Korea

(Received June 21, 2018 : revised July 7, 2018 : accepted July 10, 2018)

In most previous investigations of plasmonic and metamaterial applications, the metallic film has been regarded as a perfect electrical conductor. Here we demonstrate the resonance characteristics of THz metamaterials fabricated from metal film that has a finite dielectric constant, using finite-difference time-domain simulations. We found strong redshift and spectral broadening of the resonance as we decrease the metal's plasma frequency in the Drude free-electron model. The frequency shift can be attributed to the effective thinning of the metal film, originating from the increase in penetration depth as the plasma frequency decreases. On the contrary, only peak broadening occurs with an increase in the scattering rate. The metal-thickness dependence confirms that the redshift and spectral broadening occur when the effective metal thickness drops below the skin-depth limit. The electromagnetic field distribution illustrates the reduced field enhancement and reduced funneling effects near the gap area in the case of low plasma frequency, which is associated with reduced charge density in the metal film.

Keywords : Terahertz spectroscopy, Metamaterials
OCIS codes : (300.6495) Spectroscopy, terahertz; (160.3918) Metamaterials; (160.4670) Optical materials

I. INTRODUCTION

Metamaterials have attracted great attention lately, owing to their exotic resonance characteristics, with potential applications in cloaking [1, 2], superlensing [3], and sensing [4]. The electromagnetic behaviors of metamaterials are determined by the specific geometry of the artificial metal structures fabricated on a dielectric substrate. On the other hand, THz spectroscopy is widely used in various fields because it enables label-free, noncontact, nondestructive detection [5-10], and as a result metamaterials operating in THz frequency range have a variety of applications in safety inspection, communication, and biological and chemical sensing. The split-ring resonator (SRR) is one of the most commonly used patterns operating in the THz range, due to its simple geometry [11-16]. When the SRR structure is excited with an electromagnetic field in perpendicular polarization geometry, it exhibits an inductive-capacitive resonance (*i.e. LC* resonance), arising from the accumulation of charge in the vicinity of the SRR gap and the circular current at the side ring of the SRR.

Manipulating electromagnetic waves through structures has been realized by introducing various patterns on conventional metal films having fixed dielectric constants. Recently there have been a series of attempts to control the surrounding media by manipulating the substrate's index, rather than that of the metal film itself, through light illumination and electrical bias [16-18], for instance. On the other hand, additional freedom can be provided if the dielectric constant of the conducting film can be engineered by adjusting its internal electronic properties. Only recently, types of post-processing such as chemical treatments and nanoparticle coatings were applied to single-walled-nanotube (SWNT) and silver-nanowire (AgNW) films, resulting in considerable changes in a metal's dielectric constant [19, 20]. The resonance behaviors of the devices fabricated on the SWNT and AgNW films were modified accordingly, proving that device performance can be manipulated by

*Corresponding author: ahny@ajou.ac.kr, ORCID 0000-0002-8563-076X
Color versions of one or more of the figures in this paper are available online.

engineering the dielectric constant; however, the physical implications behind the attractive phenomena, including the resonance tuning, have not been unraveled yet.

In this report, we present finite-difference time-domain (FDTD) simulation results for the resonances of split-ring resonators fabricated from metal films with finite dielectric constants. We investigated the tuning and broadening of the resonances as a function of the plasma frequency and scattering rate of the metal. The dependence on metal thickness reveals that the reduced restoring force is responsible for the resonance change, because it is noticeable when the effective thickness is below the skin-depth limit.

II. RESULTS AND DISCUSSION

To predict the resonance frequency of the metamaterials shown schematically in Fig. 1(a), the structures were simulated using CST. Here the split-ring resonator consisted of a rectangle with outer dimensions of 36×36 μm^2 and a gap structure of distance $d = 2$ μm. The thickness and width of the metal strip were $t = 100$ nm and $w = 4$ μm respectively. The substrate's refractive index was chosen to be 1.93, corresponding to that of quartz. To focus on the *LC* resonance of the metamaterial, the simulations were performed in TM polarization geometry, as illustrated in Fig. 1(a). The material for the SRR pattern has been

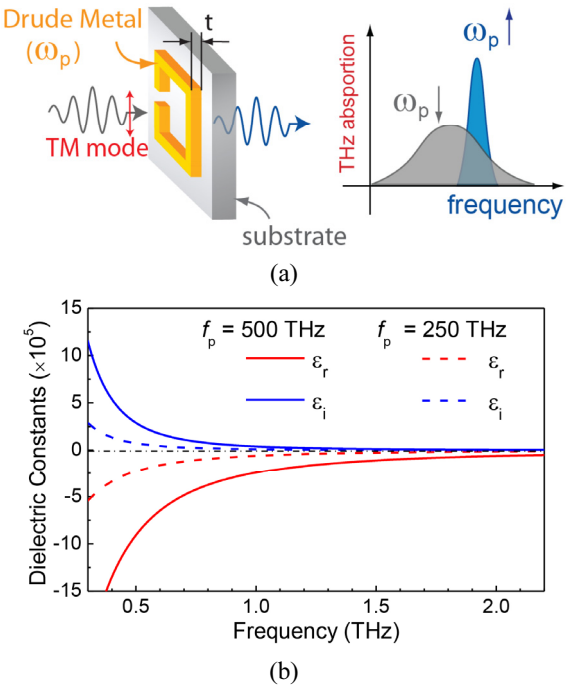

FIG. 1. (a) A schematic diagram of THz transmission through a split-ring resonator fabricated from a Drude metal film. (b) Dispersion curves for the complex dielectric constants for $f_p = \omega_p/2\pi = 500$ THz (solid lines) and 250 THz (dashed lines), for a scattering rate of $\gamma = 1$ THz.

previously considered to be a perfect electric conductor (PEC). In this work, we adopted finite metal films with dispersion relevant to the Drude free electron model; in other words, the metal's complex dielectric constant $\varepsilon = \varepsilon_r + i\varepsilon_i$ can be expressed as

$$\varepsilon = \varepsilon_\infty - \frac{\omega_p^{\,2}}{\omega^2 + i\omega\gamma}, \quad (1)$$

where ω_p is the plasma angular frequency, γ is the scattering rate, and ε_∞ is the free-space dielectric constant. The dispersion curves for ε_r and ε_i are shown as a function of frequency in Fig. 1(b) for the two different f_p (= $\omega_p/2\pi$) values.

To begin, we show in Fig. 2(a), the transmission spectra of the SRR pattern for the different plasma frequencies of the metal film in the range of 50~2000 THz. Here the scattering rate γ was fixed at 1 THz. First, the peak frequency for the PEC metal film is found to be 806 GHz, shown as a dashed line, as determined by the geometry of the pattern and also by the effective dielectric constant of the surrounding media (i.e. the combination of the indices of quartz and air) [21, 22]. The transmission spectrum that was obtained through simulation in the case of PEC metal shows good agreement with the resonant peaks found experimentally in our previous studies [21]. If we consider the finite dielectric constants of the metal films, the resonant characteristics deviate dramatically from those in the PEC case. In particular, the resonance frequency is generally lower than in the PEC case, as shown explicitly in the semilogarithmic plot of Fig. 2(b). The resonance peak for $f_p = 2000$ THz is found at $f_{res} \approx 787$ GHz, which is very close to that in the PEC case. As we decrease f_p further, the resonant frequency decreases dramatically, reaching $f_{res} \approx 300$ GHz for $f_p = 50$ THz. Importantly, it is likely that the resonant peak can be tuned continuously by adjusting the plasma frequency of the finite metal film used for the metamaterial. Indeed, the control of resonant transmission of THz waves in plasmonic and metamaterial devices has been demonstrated experimentally by engineering the dielectric constant of highly conductive SWNT and AgNW network films [15, 20].

It is also notable that the peak amplitude and width of the resonance vary with plasma frequency, as shown in Fig. 2(c). The amplitude (black squares) decreases gradually as f_p decreases, reaching as low as 0.16 when $f_p = 50$ THz, below which the resonant peak almost vanishes. This is in striking contrast to the PEC case and the case of higher plasma frequency, where the amplitude is as high as 0.85. In accordance with the reduction in amplitude, the resonance spectra spread significantly with decreasing plasma frequency. It is obvious that the penetration depth δ of the THz wave increases inversely with the plasma frequency, *i.e.* $\delta = c/\omega_p$, as plotted in the inset of Fig. 2(b). This will result in the effective thinning of the metal film, down to the skin

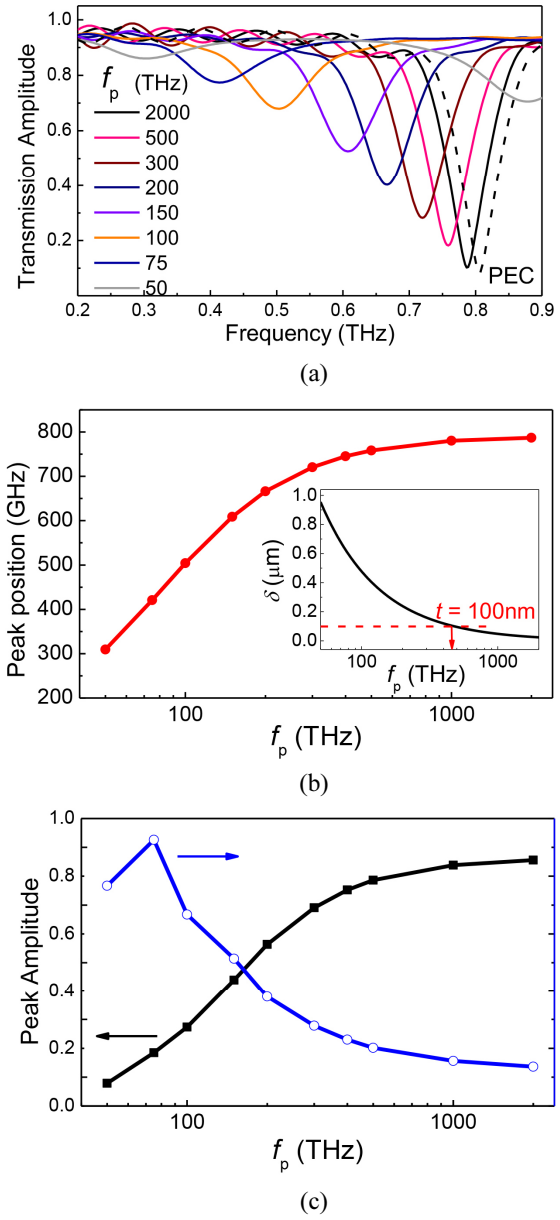

FIG. 2. (a) Simulated THz transmission amplitudes for the SRR on a quartz substrate with various f_p's from 50 to 2000 THz, for a fixed γ of 1 THz. (b) A plot of resonant peak position as a function of f_p. Inset: Calculated penetration depth as a function of f_p. (c) Peak amplitude and spectral width of the resonance as a function of f_p.

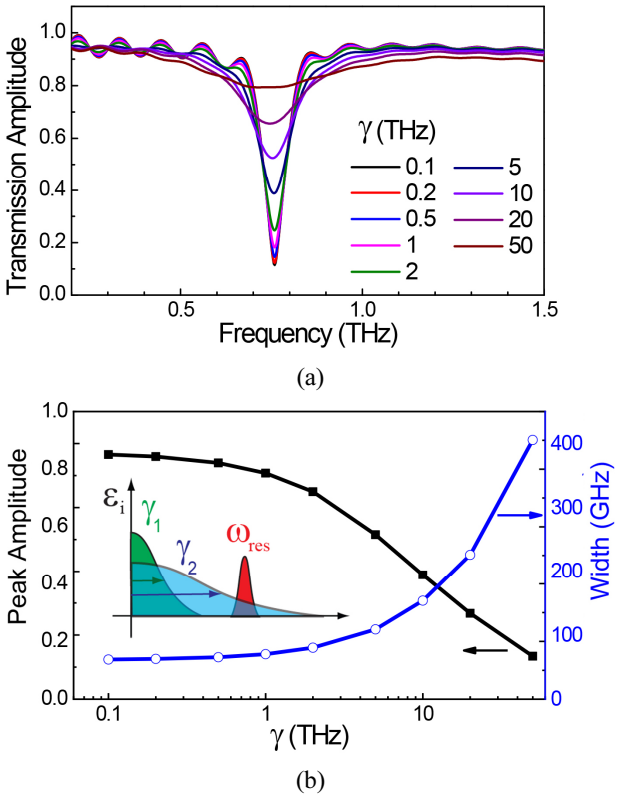

FIG. 3. (a) Simulated transmission with various γ's from 0.1 to 50 THz, for f_p = 500 THz. (b) Peak amplitude and spectral width of the resonance as a function of γ.

depth limit [23], which causes redshift of the resonance, as will be discussed later.

On the other hand, the resonance peak's position does not change significantly with the scattering rate. Figure 3(a) shows transmission amplitudes for different γ values from 0.1 to 50 THz for a fixed plasma frequency of f_p = 500 THz. Clearly, whereas the peak position remains fixed at $f_{res} \approx 780$ GHz regardless of γ value, the spectral width of the resonance broadens significantly, as summarized in Fig. 3(b). The spectral broadening accompanied by amplitude reduction can be expected simply from the large scattering rate. It is notable that the resonance suffers significant broadening especially when γ exceeds the resonant-peak angular frequency (ω_{res}), as schematically illustrated in the inset of Fig. 3(b). This is because the resonance position no longer lies in the total-reflection regime; instead, the metal film experiences absorption accompanied by Ohmic loss for $\gamma > \omega_{res}$.

To validate the thinning effects on the resonant transmission, we performed simulations for the metamaterial pattern with various metal thickness; the results are illustrated in Fig. 4. The peak position and spectral width are shown in Figs. 4(a) and 4(b) respectively, as a function of f_p, for four different metal thicknesses. The results for t = 100 nm (black squares) were retrieved from those in Fig. 2. Clearly the f_p dependence on peak position was reduced noticeably as the film thickness increased from t = 100 nm to 5 μm. This is because when the film is thicker than the penetration depth (*e.g.* δ = 0.95 μm for f_p = 50 THz, or δ = 24 nm for f_p = 2000 THz), the effective metal thickness t_{eff} is still greater than the skin-depth limit, even when the plasma frequency is low. It has been previously implied that an effective metal thickness lower than the skin-depth limit will result in the lowering of the restoring force, owing to the reduced carrier density in the metal film [24]. Therefore, the redshift of the resonance in the case of low plasma

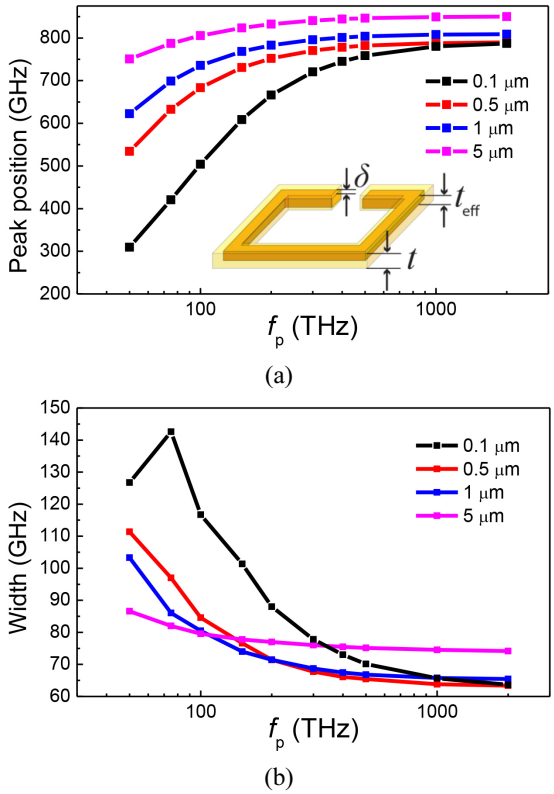

FIG. 4. (a) Resonant peak position plotted as a function of f_p for four metal thicknesses (t) of 100 nm, 500 nm, 1 μm, and 5 μm. (b) Resonance spectral width as a function of f_p for four different metal thicknesses. The results for 100 nm were retrieved from those in Fig. 2.

frequency, observed both experimentally and theoretically, can be understood in the context of the reduced restoring force.

Finally, we demonstrate the field distribution near the metal surface for two different plasma frequencies. Along the *x*-*z* plane of the schematic shown in the inset of Fig. 5, we plotted the electric field E_x at the resonance frequency for $f_p = 500$ THz (left panel) and 50 THz (right panel), at their respective resonant frequencies. For large f_p, the field distribution near the gap area clearly demonstrates the *funneling effect* associated with strong field localization near the gap structures [25]; conversely, this effect diminishes significantly for lower f_p. In addition, it is clearly seen that, accordingly, the field enhancement dramatically drops. The increased penetration depth of the THz waves into the low-conductivity metal film causes reduced charge density near the metal's gap area, followed by reduced field-enhancement effect. This is in accordance with the abrupt decrease in the resonant-peak amplitudes, as shown in Fig. 2. In other words, we will be able to control the field-enhancement factors in addition to resonant-frequency tuning by engineering the dielectric constants of the finite metal films.

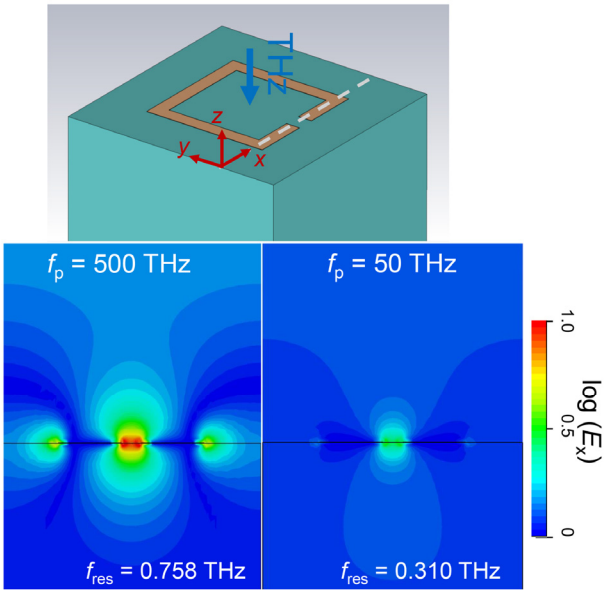

FIG. 5. Field distribution of the electric field E_x along the *x*-*z* plane (intersecting with the dashed line shown in the inset) for two different plasma frequencies $f_p = 500$ THz (left panel) and 50 THz (right panel).

III. CONCLUSION

In conclusion, we demonstrated the resonance characteristics of THz metamaterials fabricated from metal film that has a finite dielectric constant, by using FDTD simulations. Strong redshift and spectral broadening of the resonance were observed as we decreased the plasma frequency. Conversely, spectral broadening occurs without resonance shift when we increase the scattering rate. The dependence on the metal's thickness confirms that the redshift accompanied by the broadening occurs predominantly when the effective metal thickness drops below the skin-depth limit, whereas similar effects were not pronounced when the metal's thickness is much higher than the penetration depth. Therefore, the frequency shift of the resonance can be attributed to the effective thinning of the metal film associated with the reduced restoring force. In addition, electromagnetic field profiles exhibit a reduced field-enhancement effect (associated with reduced funneling effects) in the low-plasma-frequency regime. The effect of the metal's dielectric constant on the resonance frequency demonstrated in this study will provide important insight into the near-field confinement of THz waves, which is linked to resonant transmission through various subwavelength structures. Our work can be further extended to studying various nanostructures, such as nanogaps and metallic nanoantennas, in which we will find important optical and optoelectronic device applications with strong field confinement and enhancement.

ACKNOWLEDGMENT

This work was supported by the Midcareer Researcher Program (2017R1A2B4009177) through a National Research Foundation grant funded by the Korean Government (MSIP) and by the Human Resources Program in Energy Technology (20164030201380) of the Korea Institute of Energy Technology Evaluation and Planning (KETEP) grant funded by the Korean Government (MOTIE).

REFERENCES

1. D. Schurig, J. J. Mock, B. J. Justice, S. A. Cummer, J. B. Pendry, A. F. Starr, and D. R. Smith, "Metamaterial electromagnetic cloak at microwave frequencies," Sci. **314**, 977-980 (2006).
2. J. B. Pendry, D. Schurig, and D. R. Smith, "Controlling electromagnetic fields," Sci. **312**, 1780-1782 (2006).
3. J. B. Pendry, "Negative refraction makes a perfect lens," Phys. Rev. Lett. **85**, 3966-3969 (2000).
4. S. J. Park, J. T. Hong, S. J. Choi, H. S. Kim, W. K. Park, S. T. Han, J. Y. Park, S. Lee, D. S. Kim, and Y. H. Ahn, "Detection of microorganisms using terahertz metamaterials," Sci. Rep. **4**, 4988 (2014).
5. J. Federici and L. Moeller, "Review of terahertz and subterahertz wireless communications," J. Appl. Phys. **107**, 111101 (2010).
6. K. Kawase, Y. Ogawa, Y. Watanabe, and H. Inoue, "Non-destructive terahertz imaging of illicit drugs using spectral fingerprints," Opt. Express **11**, 2549-2554 (2003).
7. M. Tonouchi, "Cutting-edge terahertz technology," Nat. Photon. **1**, 97-105 (2007).
8. A. Menikh, R. MacColl, C. A. Mannella, and X. C. Zhang, "Terahertz biosensing technology: Frontiers and progress," ChemPhysChem **3**, 655-658 (2002).
9. R. M. Woodward, V. P. Wallace, D. D. Arnone, E. H. Linfield, and M. Pepper, "Terahertz pulsed imaging of skin cancer in the time and frequency domain," J. Biol. Phys. **29**, 257-261 (2003).
10. S. J. Park, A. R. Kim, J. T. Hong, J. Y. Park, S. Lee, and Y. H. Ahn, "Crystallization kinetics of lead halide perovskite film monitored by in situ terahertz spectroscopy," J. Phys. Chem. Lett. **8**, 401-406 (2017).
11. C. Enkrich, M. Wegener, S. Linden, S. Burger, L. Zschiedrich, F. Schmidt, J. F. Zhou, T. Koschny, and C. M. Soukoulis, "Magnetic metamaterials at telecommunication and visible frequencies," Phys. Rev. Lett. **95**, 203901 (2005).
12. R. Marqués, J. Martel, F. Mesa, and F. Medina, "Left-handed-media simulation and transmission of EM waves in subwavelength split-ring-resonator-loaded metallic waveguides," Phys. Rev. Lett. **89**, 183901 (2002).
13. H. O. Moser, B. D. F. Casse, O. Wilhelmi, and B. T. Saw, "Terahertz response of a microfabricated rod-split-ring-resonator electromagnetic metamaterial," Phys. Rev. Lett. **94**, 4 (2005).
14. C. Rockstuhl, T. Zentgraf, H. Guo, N. Liu, C. Etrich, I. Loa, K. Syassen, J. Kuhl, F. Lederer, and H. Giessen, "Resonances of split-ring resonator metamaterials in the near infrared," Appl. Phys. B: Lasers Opt. **84**, 219-227 (2006).
15. J. T. Hong, D. J. Park, J. H. Yim, J. K. Park, J. Y. Park, S. Lee, and Y. H. Ahn, "Dielectric constant engineering of single-walled carbon nanotube films for metamaterials and plasmonic devices," J. Phys. Chem. Lett. **4**, 3950-3957 (2013).
16. H. T. Chen, W. J. Padilla, J. M. O. Zide, A. C. Gossard, A. J. Taylor, and R. D. Averitt, "Active terahertz metamaterial devices," Nat. **444**, 597-600 (2006).
17. H. T. Chen, J. F. O'Hara, A. K. Azad, A. J. Taylor, R. D. Averitt, D. B. Shrekenhamer, and W. J. Padilla, "Experimental demonstration of frequency-agile terahertz metamaterials," Nat. Photon. **2**, 295-298 (2008).
18. S. B. Choi, J. S. Kyoung, H. S. Kim, H. R. Park, D. J. Park, B. J. Kim, Y. H. Ahn, F. Rotermund, H. T. Kim, K. J. Ahn, and D. S. Kim, "Nanopattern enabled terahertz all-optical switching on vanadium dioxide thin film," Appl. Phys. Lett. **98**, 071105 (2011).
19. J. T. Hong, D. J. Park, J. Y. Moon, S. B. Choi, J. K. Park, F. Rotermund, J. Y. Park, S. Lee, and Y. H. Ahn, "Terahertz wave applications of single-walled carbon nanotube films with high shielding effectiveness," Appl. Phys. Express **5**, 3 (2012).
20. J. T. Hong, S. J. Park, J. Y. Park, S. Lee, and Y. H. Ahn, "Terahertz slot antenna devices fabricated on silver nanowire network films," Opt. Mater. Express **7**, 1679-1685 (2017).
21. D. J. Park, S. J. Park, I. Park, and Y. H. Ahn, "Dielectric substrate effect on the metamaterial resonances in terahertz frequency range," Curr. Appl. Phys. **14**, 570-574 (2014).
22. S. J. Park and Y. H. Ahn, "Substrate effects on terahertz metamaterial resonances for various metal thicknesses," J. Korean Phys. Soc. **65**, 1843-1847 (2014).
23. R. Singh, E. Smirnova, A. J. Taylor, J. F. O'Hara, and W. Zhang, "Optically thin terahertz metamaterials," Opt. Express **16**, 6537-6543 (2008).
24. H. Guo, N. Liu, L. Fu, H. Schweizer, S. Kaiser, and H. Giessen, "Thickness dependence of the optical properties of split-ring resonator metamaterials," Phys. Status Solidi B **244**, 1256-1261 (2007).
25. J. H. Kang, D. S. Kim, and M. Seo, "Terahertz wave interaction with metallic nanostructures," Nanophotonics **7**, 763-793 (2018).